Fast method for the estimation of the absorbed dose in X-ray microtomography

Amelie De Muynck[a,*], Stijn Bonte[a,1], Jelle Dhaene[a], Manuel Dierick[a,2], Klaus Bacher[b], Luc Van Hoorebeke[a], Matthieu N. Boone[a]

[a] *UGCT - Dept. Physics and Astronomy, Ghent University, Proeftuinstraat 86; 9000 Gent, Belgium*
[b] *Department of Basic Medical Sciences, Division of Medical Physics-Gent, Ghent University, Gent, Belgium*

Abstract

Micro-CT imaging is an increasingly popular tool in the internal investigation of objects and materials. However, as an X-ray based technique, a potentially harmful radiation dose is deposited in the sample during the measurement. In (non small-animal) micro-CT imaging one is dealing with a strong variation in measurement systems and settings, resulting in many different acquisition circumstances and the absence of standard imaging protocols. Therefore, the deposited dose is rarely studied for micro-CT applications. This research aimed at developing a fast simulation technique to predict the dose associated with micro-CT scanning. Its performance is compared with that of two different Monte Carlo simulation tools and with a straight forward approach to estimate an upper limit for the dose. The fast simulation method, obtaining a dose estimation based on the energy absorption coefficient, is much faster than the Monte Carlo simulations, and the results are accurate within 30%. This enables us to predict the dose for a known sample and a known scanner setup, without complex Monte Carlo simulations and will allow researchers to avoid radiation damage or unwanted radiation induced effects, an increasingly important concern in 3D and 4D micro-CT scanning.

*Corresponding author: E-mail Amelie.DeMuynck@UGent.be; Tel +32 9264 6611; Fax +32 9264 6697

[1] Present address: Medical Imaging and Signal Processing (MEDISIP), Dept. Electronics and Information Systems, Ghent University, IBiTech - Campus Heymans - Block B, De Pintelaan 185, 9000 Gent, Belgium

[2] Present address: XRE nv, Bollebergen 2B box 1, 9052 Gent, Belgium

1. Introduction

High resolution X-ray computed tomography (micro-CT) is an increasingly popular technique for non-destructive internal sample visualisation. A drawback of X-ray imaging is the deposition of a radiation dose in the object being imaged. For medical applications, it is important to quantify and minimize this dose, because it can be harmful to the patient's health. In comparison to medical scans, micro-CT scans have a much higher resolution, hence a smaller voxel size, which typically gives rise to a higher dose in the object under investigation [1, 2]. For a given material, the absorbed dose scales roughly linearly with the number of interactions per unit of volume, hence for a fixed signal to noise ratio the dose will scale as (voxel volume)$^{-1}$. In medical CT, the degrees of freedom are strongly limited by the available protocols implemented by the manufacturer. These standardised protocols facilitate the dose calculation and verification by means of phantoms with incorporated dosimeter(s), because only a limited amount of combinations of the degrees of freedom need to be studied. In modern micro CT systems, the source-object distance (SOD) can be varied and is an additional degree of freedom, as well as the scan time and the type of source. Furthermore, micro-CT can be used in a large number of research domains, and the objects under investigation can vary strongly in size and composition, hence no standardized protocols are available and for smaller objects, incorporating dosimeter probes without affecting the dosimetric behaviour is typically impossible. The variety of setup properties, acquisition settings and sample composition make standardized dosimetry tests very difficult to define and perform.

Due to the differences between micro-CT and medical CT, the standardized dosimetry calculations and measurements of medical applications cannot be applied in micro-CT scans. For practically all applications of micro-CT, except for small animal micro-CT scanners [3, 4, 5, 6, 7], very little information is available in literature about dose deposition in the samples. Occasionally, the dose in a sample is mentioned as background information [8], but the reliability of these values is limited because it is almost never specified how this dose is obtained. In some cases, the dose is measured [9] or calculated [10, 11], though even in these cases the validity of the measurement or

2

calculation is not investigated. For a large number of applications, the dose is of minor importance, because the sample will not be affected by the dose involved in laboratory-based micro-CT. However, some samples are radiation sensitive. A first example are materials of which the colour can change due to radiation [12]. A second example are plants which need to be examined several times during their lifetime. Although plants do not necessarily die, their growth can be stopped or suspended by the radiation [13]. These two examples indicate that it can be important to have a good approximation of the deposited dose that the sample under investigation will receive during the total scan time. The International Commission on Radiological Protection (ICRP) already studied the relation between absorbed dose and damage in fauna and flora [14]. In addition, the increasing popularity of 4D scans with long exposure times arouses interest for dose estimations among researchers in the microtomography community. Monte Carlo simulations are a strong tool to calculate the expected dose in a sample, but their biggest drawback is that those simulations are time-consuming. Therefore, the aim of this study is to provide a fast and sufficiently accurate method (roughly within a factor of 2 of accuracy) for the present purpose. The obtained results are compared with two different Monte Carlo simulation tools. These results can for example be used to be correlated with observed radiation induced effect patterns [15].

2. Materials and methods

2.1. The proposed dose estimation method

The proposed method, referred to as the μ_{en}-method, divides the materials between the source and the object under investigation (which is usually (part of) the sample) in slabs, perpendicular to the X-ray beam axis. These slabs are called material slabs and can represent actual filter materials, air and sample materials. The dose is calculated in the last material slab, which we call the relevant sample slab and corresponds to (a part of) the sample. In front of the relevant sample slab, the X-ray beam is attenuated in the material slabs.

The dose, D, is defined as the deposited energy, E_{dep}, in a volume divided by the mass of that volume, m:

$$D = \frac{E_{dep}}{m}.$$

(1)

The used volume for E_{dep} and m is that of a cube with the thickness of the relevant slab as edge length. The unit of dose is Gray (Gy), which corresponds to 1 Joule per kilogram. A user-defined X-ray energy spectrum is used for energy dependent X-ray beam attenuation calculation. The source spectrum is divided in energy bins as described in [16]. A parallel beam is assumed, and the limits of this assumption are explored in section 3.2. For every energy bin, the general calculation process is:

1. In every material slab prior to the object under investigation the beam is attenuated according to the law of Lambert-Beer using the linear attenuation coefficient, μ, of the specified material. The material slabs can correspond with filters used for beam filtration, that are mostly positioned close to the source and far from the sample. They can also correspond with a part of the object if the main interest is the dose in a subsequent part deeper in the object i.e. the already above mentioned 'relevant slab'.
2. In the relevant sample slab, the dose is calculated by using the energy absorption coefficient, μ_{en}, which allows to determine the amount of energy deposited in a layer [17]. Only one material slab of interest can be specified in this method.

At the end, the contributions of all energy bins are summed.

In the material slabs, every photon that interacts through photo-electric absorption or Compton scattering is removed from the beam. The scattered photons that will in reality eventually reach the relevant sample slab are thus ignored. In section 3.3 we investigate the effect of ignoring these scattered photons. In this approach the Rayleigh scattered photons are neglected, which is a good approximation because the direction of the photon is only slightly changed, and the photon can leave the slab with its original energy. More information on the different interaction mechanisms of X-rays can be found in [18].

In the relevant sample slab the dose is calculated using the energy absorption coefficient, μ_{en}. These energy absorption coefficients are defined for infinitely thin slabs and allow to calculate the transmitted intensity of an X-ray beam, whereby only the energy of the secondary electrons produced in the interaction processes is deposited in the slab. The difference between the linear attenuation coefficient and the energy absorption coefficient for water is shown in figure 1. Especially in the energy range used in micro-CT, the

4

difference becomes significant. As μ_{en} is defined for infinitesimal thin layers, the influence of slabs with finite thickness will be investigated in section 3.1
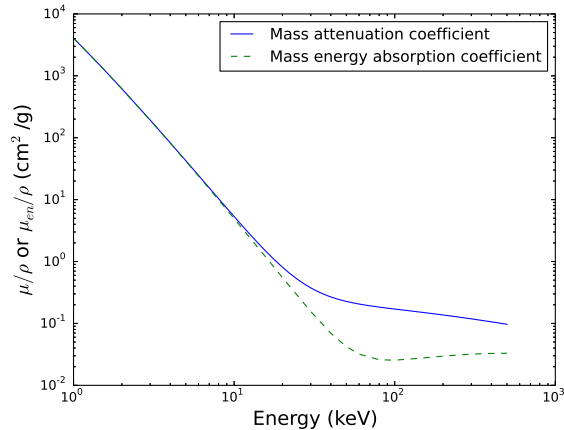

Figure 1: Comparison between the mass attenuation coefficient and the mass energy absorption coefficient for water as a function of the photon energy. The μ/ρ and μ_{en}/ρ values are taken from the current photon interaction database at the National Institute of Standards and Technology [19].

The fast method is developed in the framework of an in-house developed tool for polychromatic X-ray transmission calculation dubbed Setup Optimiser, part of the CT projection simulation framework ARION [16]. The framework is based on the law of Lambert-Beer to calculate the measured attenuation of a polychromatic X-ray beam through an object using a high-precision Monte Carlo modellation of the tube X-ray energy spectrum and polychromatic detector response. The geometry is simplified to a series of consequent slabs with a given thickness of a specific material. As the method presented here uses the same slab approach, it was convenient to be incorporated in the Setup Optimiser as an extension.
Next to the proposed method, the linear attenuation coefficient in the relevant slab can also be considered to calculate the dose. However, it is obvious that this latter dose is in most cases an upper limit for the actual deposited dose since the total energy of all interacting photons is locally deposited, i.e. the energy escape from the interaction volume due to for example Compton scattering and fluorescent X-rays is not taken into account. This effect is

5

stronger for high-energy photons, and in this approach Rayleigh scattered photons are also neglected. This dose can be referred to as the "total deposition" dose and will be useful in the remainder of this paper for the interpretation of the results of the fast method and the Monte Carlo simulations.

2.2. Monte Carlo simulations

The Monte Carlo simulations were performed using BEAMnrc [20] and Geant4 [21], two simulation tools that have already been compared for a wide range of applications [22, 23, 24, 25, 26, 27]. BEAMnrc is a software tool to model radiation beams using EGSnrc (electron gamma shower) developed by the National Research Council Canada. EGSnrc is used to address a broad range of questions about the propagation of radiation in materials. It is particularly well-suited for medical physics purposes, but given its flexible, modular design and companion utilities, EGSnrc can also be used for a vast range of other applications, including the simulation of research and industrial linac beams, X-ray emitters, radiation shielding, and more [20]. Geant4 is another toolkit for the simulation of the passage of particles through matter. It is developed at CERN and its areas of application include high energy, nuclear and accelerator physics, as well as studies in medical and space science [21]. In Geant4 we used a reference physics list, which guarantees usage of a well-validated combination of physics models. The chosen list was 'QBBC', which contains both the electromagnetic and hadronic physics processes. Both Monte Carlo simulations take into account Compton scattering, Photo-electric effect, Rayleigh scattering, Bremsstrahlung, atomic relaxations and multiple electron scattering.
To optimize the efficiency of the simulations with a cone beam, the opening angle of the simulated beam is chosen such that the complete object is irradiated by the beam and only a minimum of the generated photons will never hit the object. The used beam parameters for each geometry are mentioned in section 2.4. All simulations are performed with a total of 10^8 photons present in the simulated beam, to reduce the uncertainty of the dose simulation results below 0.5% and limit the simulation time.

2.3. Spectral properties

The performed simulations are based on the geometry of HECTOR [28], one of the scanners at the 'Centre for X-ray Tomography' of Ghent University (UGCT; www.ugct.ugent.be [29]). This system is a custom-built and flexible high resolution X-ray CT scanner, developed in collaboration with

the spin off company XRE (`www.xre.be`, presently part of TESCAN). Due to its high flexibility and large range of tube voltage (20-240 kV) and image resolution (3-200 μm), this setup has become the work horse of the facility and is used in a wide variety of applications [e.g. 30, 31, 32, 33, 13]. Furthermore, the main components which make up this system, notably an X-RAY WorX X-ray tube with a tungsten target, have well-known properties provided by the manufacturers, which allows for detailed component simulations. The X-ray beam energy spectrum used in the simulations is the beforehand simulated output energy spectrum of the X-ray tube of HECTOR, simulated with BEAMnrc as described in [16]. For every possible tube voltage, the spectrum is simulated once, and all obtained spectra are stored in a spectrum library. An example of simulated X-ray spectra can be seen in figure 2. All simulation methods (μ_{en}, BEAMnrc and Geant4) make use of the same simulated X-ray energy spectra.
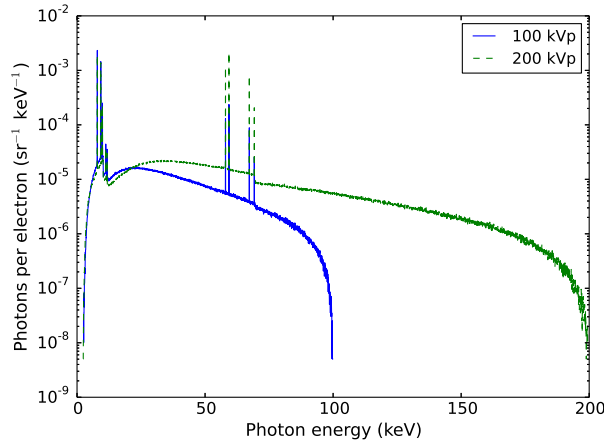

Figure 2: Simulated spectra with peak voltage 100 and 200 kVp of the X-ray source of HECTOR. The simulations are performed with BEAMnrc and the workflow is experimentally verified (unpublished data).

2.4. Evaluated geometries

Four different tests, reflecting the effect of variation in sample size and composition, beam geometry and sample shape, scattering processes and the slab approach to describe filters and samples were performed. They are conceived to gain a better insight on the influence of different degrees of freedom as they are commonly used in X-ray micro-CT scanning.

7

1 To study the effect of the sample dimensions and composition, a cube of a given material (air, water, silicon dioxide or iron, which represent the actual spectrum of materials scanned in micro-CT X-ray imaging) with different dimensions was used as sample. The edge lengths of the cubes were 0.1, 0.2, 0.5, 1, 2, and 5 cm and they were positioned with their side facing the source at 5 cm from the X-ray source in vacuum. Because of the vacuum, the photons can only interact in the cubes, which excludes the possible effects from the surrounding materials. All simulations were performed with a parallel beam with a square cross-section with the same dimensions as the sample. The used X-ray spectrum of 100 kVp and 50 W target power of a directional tube [28] was already shown in figure 2. The parallel beam covers the complete sample and is chosen here to exclude cone beam effects. Indeed, in a cone beam there is a variation of path lengths through the sample contrary to a parallel beam. This gives the opportunity to examine the correctness of the results of the slab approach, without including errors due to different path lengths.

2 To study the effect of beam geometry and sample shape, in the second test two sample shapes were considered, a cube with edge length 1 cm and a cylinder with height 1 cm and radius 0.5 cm, both made of SiO_2, representing a geological material. The surrounding material was vacuum. The chosen tube settings were a cone beam with tube voltage of 100 kVp and tube power of 50 W. The distance between the source and the front of the object was ranging from 0.5 to 50 cm, to quantify the induced effect caused by the different path lengths of photons from a cone beam. For the smallest distances, the mean path lengths will differ significantly between photons of a parallel beam or a cone beam. For the largest source-object-distance, the mean path length in the sample will not differ largely for the two beam geometries. The opening angle of the cone was chosen in such a way that the complete object was irradiated. The opening angle was ranging from 110° for a distance of 0.5 cm between source and object to 1.7° for a distance of 50 cm. The photons were isotropically emitted within the cone, thus ignoring the heeling effect. This assumption is valid because for CT scanning this effect will be averaged during a rotation.

3 To examine the influence of scattered photons, the third geometry was a 1 cm water cube with a filter in front. Vacuum was again used as surrounding material. The distance between the source and the object was 50 cm, but the distance between the sample and the filter was ranging from 0 to 30 cm. The simulations were performed with a filter of 1 mm Al on the one hand and 1 mm Cu on the other hand. The tube settings were 100 kVp and 50 W. The cone opening angle was 2° and the photons were isotropically emitted within the cone. The geometry is shown in figure 3.
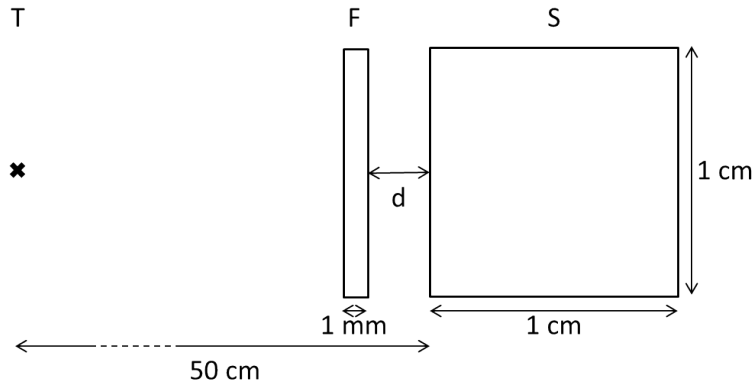

Figure 3: A transversal view of the used geometry. The distance between the X-ray source (T) and the sample (S) is fixed. The distance (d) between the filter (F) and the sample is ranging from 0 to 30 cm.

4 To evaluate the correctness of the simplified geometry consisting of layers in the μ_{en}-method, a more complex sample was used. The dose deposition was studied in a carbon cylinder inside a wooden wall, mimicking a pencil. The radius of the carbon tube was 1 mm and the thickness of the wooden wall was 2.5 mm. The height of the cylinder was 10 cm and the centre of the object was positioned at 20 cm from the source. To make the simulations as realistic as possible, the cylinder was positioned in air. The geometry is shown in figure 4. The simulations were performed with different tube spectra, ranging from 20 to 200 kVp, in steps of 10 kVp. The tube current was kept constant at 0.5 mA, resulting in a range of powers from 10 W for 20 kVp to 100 W for 200 kVp. The cone opening angle was 30° and the direction of the

simulated photons was isotropically spread. In the μ_{en}-method, a slab of 19.65 cm air and a slab of 2.5 mm wood were used as material slabs and the object was a slab of 2 mm carbon (previously referred to as the relevant slab).
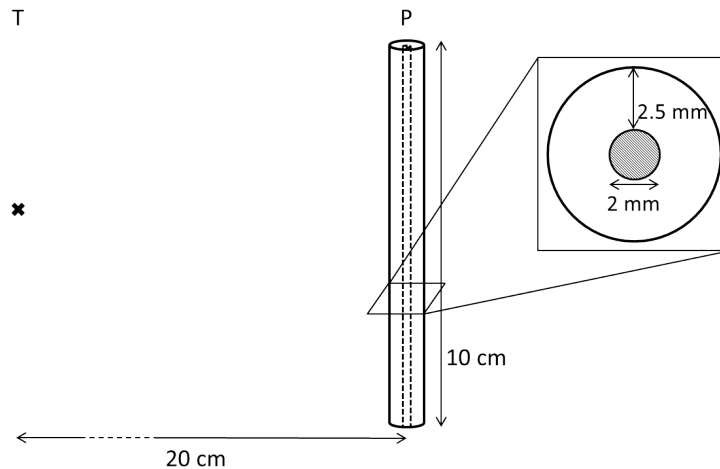

Figure 4: A schematic view of the used geometry. The X-ray source is denoted by T and the pencil phantom by P.

Analogous simulations were performed with more dense materials. The used geometry was a limestone sphere with a diameter of 1 cm with a spherical diamond inclusion with a diameter of 1 mm. For this geometry, only Geant4 is used as Monte Carlo tool because spherical objects are not included in the standard BEAMnrc package.

3. Results and Discussion

3.1. Dimension of the sample

Simulations of the dose deposition in cubes with different dimensions consisting of 4 different materials (air, water, silicon dioxide and iron) were performed. The results are shown in figure 5, where the dose averaged over the sample volume is plotted against sample size. It must be noted that the dose is not deposited homogeneously over the sample volume and the local dose deposition follows in first order the exponential attenuation of the beam through the sample. Particularly for highly attenuating materials the

10

local dose deposition can be much larger than the average. However, the study of this local dose deposition is rather complex and out of the scope of this work. Furthermore, in X-ray CT this heterogeneous dose deposition is typically less pronounced with increasing transmission and also the rotational movement of the sample yields an averaging effect. As an extra indication the transmission for some sample sizes is added in figure 5. The higher the transmission, the more homogeneous the dose will be.
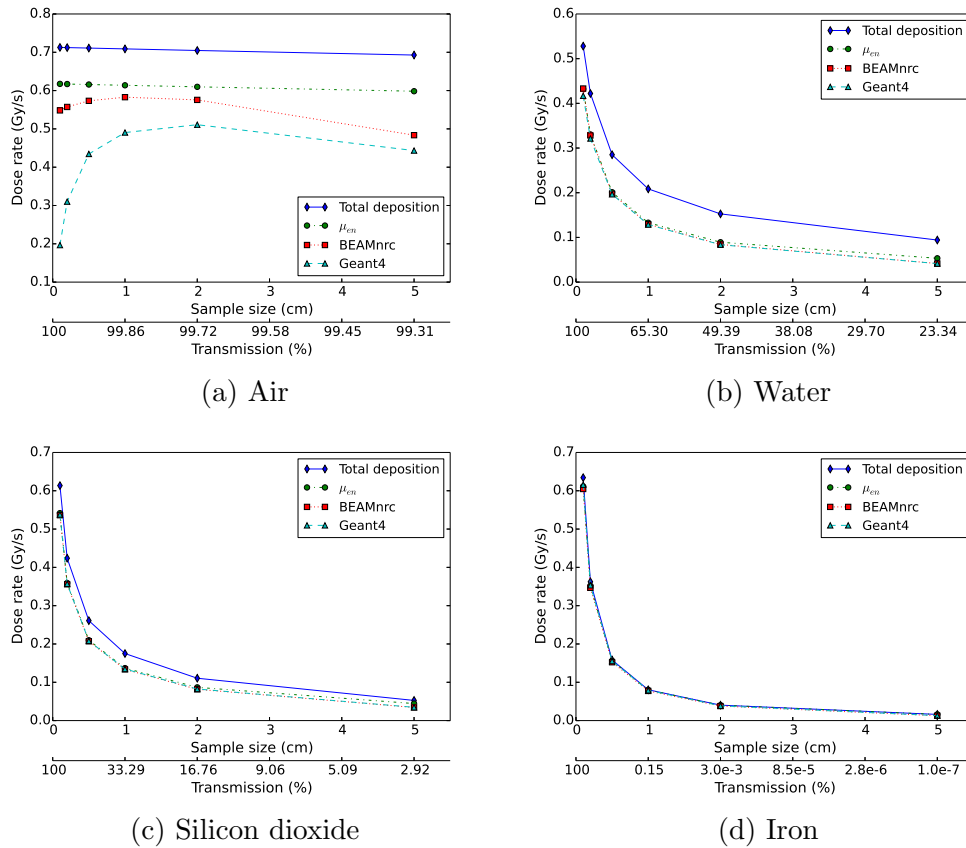

(a) Air (b) Water

(c) Silicon dioxide (d) Iron

Figure 5: Mean dose rate as function of the sample size. The tube voltage was 100 kVp and the tube power 50 W. The distance between the source and the front of the object was 5 cm. Note that the transmission axis is not linear.

For the simulations in water, silicon dioxide and iron, the mean dose decreases as function of the sample size. This decrease is due to the exponential

11

Table 1: The average path length travelled by an electron as it slows down to rest, calculated in the continuous-slowing-down approximation (CSDA-range). This data is taken from the NIST database [34].

Energy (keV)	CSDA-range (mm)			
	Air	Water	SiO_2	Iron
20	8.12	0.0086	0.0047	0.0018
80	92.12	0.0977	0.0518	0.0187
125	196.02	0.2083	0.1097	0.0392

beam attenuation in the sample. Only for the simulations of the air cubes, all simulation techniques yield a different behaviour. The Geant4 simulations clearly show a dose build-up effect. The range of this effect is a result of the mean free path of secondary electrons. In air, those particles can travel a significant distance before depositing all their energy, as shown in table 1. For all other materials the range of the dose build-up is much smaller than the scale we look at.

The simulation of BEAMnrc also indicates a dose build-up, however the effect is significantly smaller. It is therefore clear that BEAMnrc and Geant4 cope differently with secondary electrons. Only in the rather rare situation of such an extreme manifestation of dose build-up, this results in large variations between the two Monte Carlo simulations. For all other materials the difference between those two simulation tools are negligible for the scales looked at. The μ_{en}-method and the total deposition method do not take electron transport and photon scattering into account, so dose build-up is not observed for those simulations. Figure 6 shows the results normalised on the total deposition method as this curve can be determined analytically and is easy to interpret.

The first conclusion we can make is that the two Monte Carlo techniques yield the same results (except for air as discussed above). We also see that the Monte Carlo simulations always yield clearly lower doses than the total deposition method, even without Rayleigh scattered photons included in the latter. Note that both Monte Carlo tools do include Rayleigh scattering.
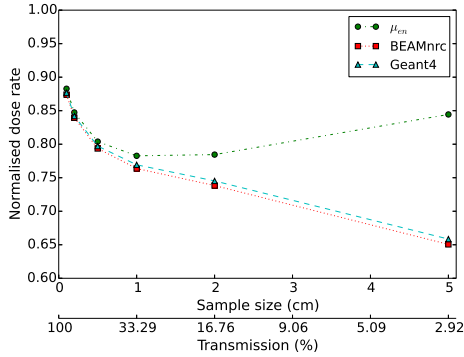
Secondly, we can conclude that the energy absorption coefficient method approaches the total deposition value for objects with low transmission thus high absorption. Nearly all photons are absorbed in the material resulting in the same average dose estimation.
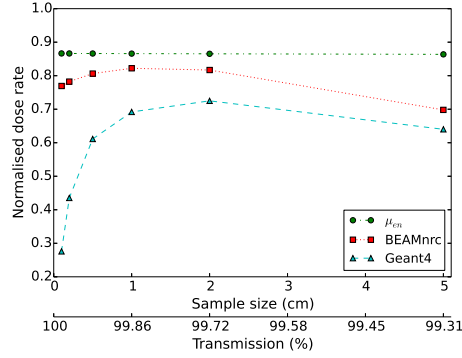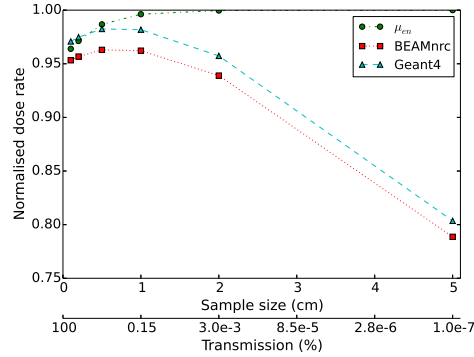
(a) Air
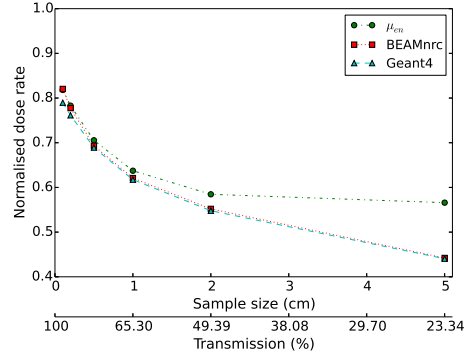
(b) Water

(c) Silicon dioxide

(d) Iron

Figure 6: Normalised dose rate as function of the sample size. The same data as shown in figure 5 is used for this figure. Note that the normalised dose correponds with the normalised deposited energy.

A last conclusion is that the energy attenuation coefficient method shows good agreement with the Monte Carlo simulations for relevant object sizes. Except for the simulations in air, the difference between the energy absorption coefficient method and the Monte Carlo simulations is maximum 30%. The behaviour of the results of the Monte Carlo simulations with respect to those obtained with the methods based on energy- and linear attenuation coefficients is a complex interplay of material and sample size, which determine the ratio of photoelectric absorbed over Compton scattered photons and the mean path length of the X-ray photons, thus the surface and depth from which photons can be scattered from the sample. All these effects are

13

Table 2: The computation time of the different simulation methods, all performed on a normal desktop computer.

	μ_{en}	BEAMnrc	Geant4
Air	104 ms	53.8 s	1670.8 s
Water	104 ms	528.1 s	1887.8 s
SiO_2	104 ms	1914.5 s	2009.3 s
Iron	104 ms	6641.3 s	2042.4 s

taken into account in the Monte Carlo simulations. The same simulations have been performed for a spectrum of 20 and 200 kVp and the results show comparable trends at lower and higher atomic number of the materials, respectively (the results can be found in the supplementary figures). E.g.: the trend for the simulations of the silicon dioxide cubes with a spectrum of 20 kVp is the same as for the iron cubes at 100 kVp. For higher energies the difference between the total deposition method on the one hand and the three simulation methods on the other hand becomes larger. Especially high energy photons are able to escape after (multiple) scattering from the volume and thus the assumption that all the interacted photons will deposit their complete energy is less correct for high energy spectra in comparison to spectra with a low end point energy.

Next to the obtained results, also the computation times can be compared. In table 2 the simulation times for the different methods is compared for the simulations of the cubes with edge length of 1 cm. The other dimensions will give similar results. All simulation methods are performed on a standard desktop computer. It is immediately clear that the μ_{en}-method is some orders of magnitude faster than the two Monte Carlo simulations. Note that the time for setting up the simulations is not included.

3.2. Effect of the cone beam geometry and sample shape

According to section 3.1 the fast estimation method (μ_{en}) gives sufficiently accurate dose estimations for parallel beams. To study the effect of a cone beam on the results, the SOD is varied, while two sample geometries are simulated to study the sample shape effect: a cube of SiO_2 with edge length 1 cm and a cylinder of SiO_2 with height and diameter 1 cm. By increasing the source object distance, the corresponding opening angle of the cone hitting the sample decreases and the cone beam geometry approaches more and more the parallel beam geometry. As expected, the dose obtained in cone beam

geometry scales with a factor $1/SOD^2$. The results are shown in figure 7 and are normalised to the total deposition method to compensate for the $1/SOD^2$ factor and make the difference between the different simulation techniques clearly visible.
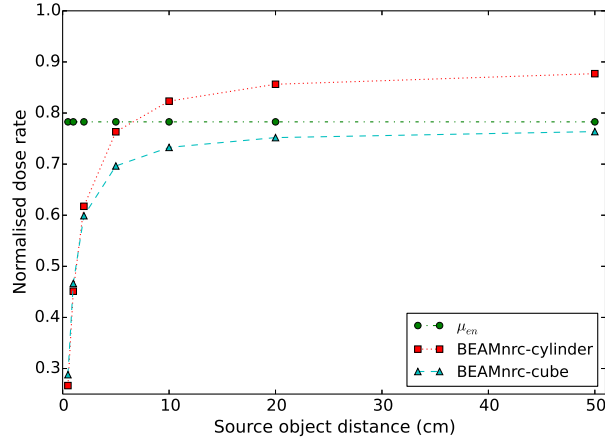

Figure 7: Normalised dose rate as function of the source object distance. The used tube voltage was 100 kVp. For visibility reasons, only the Monte Carlo results for both the cube and cylinder obtained with BEAMnrc are shown as the difference between these and the Geant4 results was negligible. The results shown for the μ_{en}-method and the total deposition approach apply to both sample shapes, because every sample shape is simplified as a slab.

For the μ_{en}-method and the total deposition approach, these two sample geometries are exactly the same because they are modelled identical in the slab approach. However, it is clear that the Monte Carlo calculated dose in the cylinder is higher than in the cube as the cylinder is - on average - smaller (see observed trends in figure 5). This indicates that the mean path length of the photons is smaller in the cylinder than in the cube and the average beam intensity through the sample is therefore larger for the cylinder. It was checked that for both sample geometries the simulation with a source object distance of 50 cm gives the same results as a simulation with a parallel beam. The size of the induced deviation due to the cone beam will be dependent on the specific cone angle. Especially for large solid angles, and thus small source object distances, the results calculated with the slab approach are less reliable. As an example, the aforementioned system HECTOR typically has

a cone opening angle of 30°, corresponding with an SOD of 2.64 cm for a cube with edge length 1 cm. From figure 7 it can be seen that for an SOD of 2.64 cm, the dose will be lower than determined with the μ_{en}-method. The deviation between the results of an opening angle of 30° and the results of a quasi parallel beam is approximately 20%.

3.3. Effect of scattered photons

Figure 8 shows the dose rate as function of the distance between the filter and the sample. For the μ_{en}-method, each distance results in exactly the same dose estimation, because photon scattering effects are not included. For the Monte Carlo simulations, each data point is the result of a different simulation with a different geometry.

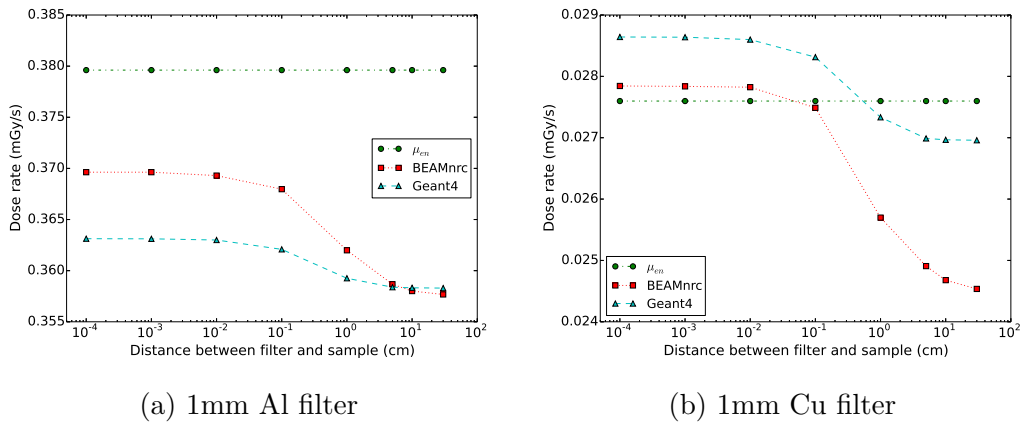(a) 1mm Al filter   (b) 1mm Cu filter

Figure 8: Dose rate as function of distance between filter and sample. The distance is plotted on a logarithmic scale to include the filters positioned both far away from the sample (at the source) and close to the sample. The used tube settings are 100 kVp and 50 W.

For small distances, the dose is almost constant, because all photons that are scattered from the filter in the forward direction will reach the sample. For large distances the dose is also constant, because almost none of the scattered photons will reach the sample. The tipping point occurs when the distance between the filter and the sample is of the same order of magnitude as the dimension of the sample. Although there is a relation between dose and distance between filter and sample, the effect is relatively small, which proves that the results will be barely influenced by neglecting the scattered

16

photons in the filters. The maximal deviation between μ_{en}-method and the Monte Carlo simulations is 12.5%.

3.4. Simplification of complex geometries

The results of the simulations mimicking the pencil are shown in figure 9a. In general, the total deposition approach gives an upper limit for the dose, as expected. The larger the tube voltage, the larger the overestimation is, due to the increasing importance of Compton scattering. However, for the smallest tube voltage of 20 kV, the total deposition method underestimates the Monte Carlo simulations by approximately 4%. This is caused by the photons scattered in the wooden wall, that will reach the carbon tube and deposit their energy. These scattered photons are removed from the beam in the total deposition method and in this particular case, they play a non-negligible role.
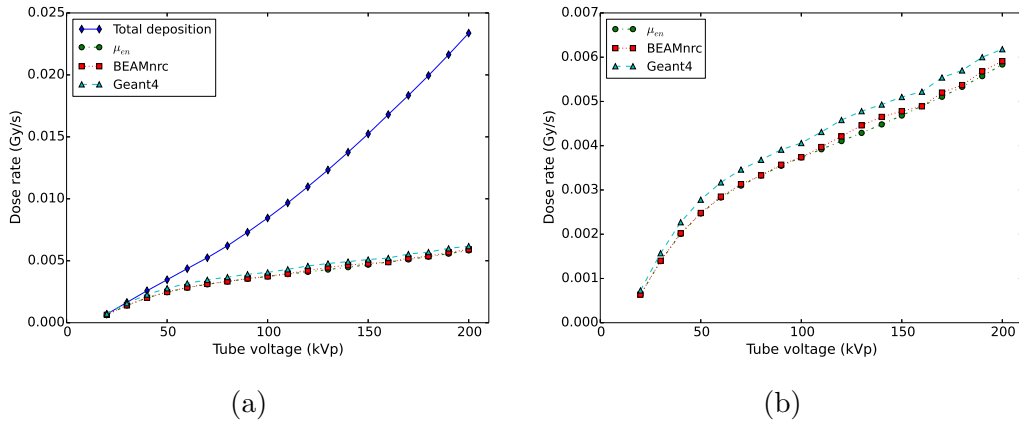

Figure 9: Dose rate in the pencil as function of the tube voltage. A constant tube current of 0.5 mA is used. a) The four different simulation methods are displayed. b) The three relevant simulation methods are shown.

To take a closer look to the three other simulation techniques, the same results are plotted without the total deposition method in figure 9b. The results of both Monte Carlo techniques differ on average by 8%. The simulation method with the energy absorption coefficient is closely following the BEAMnrc simulations and differs maximally 14% from the Geant4 simulations.

The results are analogous for the limestone sphere with a diamond inclusion. Again, for the smallest tube voltage, the total deposition method gives

an estimation below the results of the Geant4 simulations. The difference between the energy absorption coefficient method and the Geant4 simulations is about 17%. This deviation is larger than for the pencil geometry, because for a spherical inclusion the available surface from which scattered photons can enter the inclusion is also larger. As such, also for complex geometries, not consisting of layers, simulations with a simplified geometry can give useful approximations.

3.5. Limitations of the used techniques and future improvements

The different simulation techniques all have their own specific shortcomings. The biggest drawback of BEAMnrc is that the user has to make use of predefined geometrical shapes. This makes it difficult and sometimes even impossible to perfectly mimic the real geometry. In contrast to BEAMnrc, it is possible with Geant4 to use a random geometry. The user has to specify this geometry with a Geometry Class written in C++. Therefore, the defining of the geometry is more flexible but also more time-consuming in Geant4 than in BEAMnrc. The Monte Carlo simulations are also the most time-consuming technique. One simulation using a prior calculated beam spectrum takes on average 10 minutes, although the simulation time strongly depends on the used materials and tube voltage. Every Monte Carlo simulation presented in this manuscript is performed with 10^8 photons in the beam, without variance reduction techniques resulting in an estimated dose with an error smaller than 0.5%. Typically, simulations with high Z materials and a spectrum with a high tube voltage cause longer simulation times than the opposite situation. The dose simulations performed with the energy attenuation coefficient are calculated on the fly.

The geometrical argument is also valid for the μ_{en}-method. The user can only specify different layers without any geometrical information. A second drawback of the proposed method is that the energy attenuation coefficient is defined for infinitely small sample sizes and is thus an approximation for most realistic sample sizes. Additionally, in the material slabs every photo-electric or Compton interacted photon will be removed from the X-ray beam. This also causes scattered photons to disappear at the interaction point, but in reality they mostly travel a certain distance before depositing their energy. Thus far the dose averaged over the sample is studied in a static situation. In reality, the dose is deposited heterogeneously throughout the sample. Furthermore, in tomography the object rotates, which makes dose calculations more complex. However, as already mentioned in section 3.1 the averaging

over the sample already compensates up to some extent for the rotational movement. For a homogeneous object the dose rate should be multiplied by the scan time to obtain the dose during the total scan, provided that the attenuation is not too strong. This method is not suited for non-homogeneous objects e.g. radiation sensitive inclusions in a larger object. Taking the rotation into account in more detail and studying the local dose deposition are future goals.

Up to now, a fast simulation technique is developed and compared with two Monte Carlo techniques. All the assumptions and simplifications are extensively tested. The next step is to compare these simulations with measurements performed at our CT-scanners.

4. Conclusion

In this paper, a fast dose simulation method is presented and compared with two different Monte Carlo simulation programs, BEAMnrc and Geant4, and with a total deposition approach to estimate an upper limit for the dose. The results of the two Monte Carlo simulations are mostly comparable. The drawback of these simulations is that the preparation and execution of the simulations make them time-consuming. We show that it is possible to calculate an estimation for the dose based on the energy absorption coefficient. For most geometries this latter method gives sufficiently accurate results for the applications of micro-CT scanning, for which an accuracy of a factor of 2 is typically sufficient. With this method, an error even smaller than 30% is achieved for realistic objects and scanning parameters. This will enable researchers in various fields to study the effects of radiation, hitherto impossible due to the absence of quantitative measurements of the exposed dose.

The most important advantage of the fast simulation method is that the results are immediately obtained. All simulation methods, except Geant4, have the same drawback: a rather limited flexibility to describe the sample in which to simulate the dose deposition. Future goals are to expand the techniques to a rotating sample instead of a static sample, studying the local dose deposition and to compare the simulations with actual experimental results.

Acknowledgements

References

[1] C. Jacobsen, Future challenges for x-ray microscopy, in: XRM 2014: Proceedings of the 12th International Conference on X-Ray Microscopy, Vol. 1696, AIP Publishing, 2016, p. 020035.

[2] M. R. Howells, T. Beetz, H. N. Chapman, C. Cui, J. Holton, C. Jacobsen, J. Kirz, E. Lima, S. Marchesini, H. Miao, et al., An assessment of the resolution limitation due to radiation-damage in x-ray diffraction microscopy, Journal of electron spectroscopy and related phenomena 170 (1) (2009) 4–12.

[3] H. Li, H. Zhang, Z. Tang, G. Hu, Micro-computed tomography for small animal imaging: technological details, Progress in natural science 18 (5) (2008) 513–521.

[4] S. C. Lee, H. K. Kim, I. K. Chun, M. H. Cho, S. Y. Lee, M. H. Cho, A flat-panel detector based micro-ct system: performance evaluation for small-animal imaging, Physics in Medicine & Biology 48 (24) (2003) 4173.

[5] S. A. Detombe, J. Dunmore-Buyze, I. E. Petrov, M. Drangova, X-ray dose delivered during a longitudinal micro-ct study has no adverse effect on cardiac and pulmonary tissue in c57bl/6 mice, Acta Radiologica 54 (4) (2013) 435–441.

[6] C. T. Badea, S. M. Johnston, Y. Qi, G. A. Johnson, 4d micro-ct for cardiac and perfusion applications with view under sampling, Physics in Medicine & Biology 56 (11) (2011) 3351.

[7] R. Taschereau, P. L. Chow, A. F. Chatziioannou, Monte carlo simulations of dose from microct imaging procedures in a realistic mouse phantom, Medical physics 33 (1) (2006) 216–224.

[8] H. Cochard, S. Delzon, E. Badel, X-ray microtomography (micro-ct): a reference technology for high-resolution quantification of xylem embolism in trees, Plant, cell & environment 38 (1) (2015) 201–206.

[9] J. Van den Bulcke, M. Boone, J. Van Acker, L. Van Hoorebeke, Three-dimensional x-ray imaging and analysis of fungi on and in wood, Microscopy and Microanalysis 15 (05) (2009) 395–402.

[10] S. Zappala, J. R. Helliwell, S. R. Tracy, S. Mairhofer, C. J. Sturrock, T. Pridmore, M. Bennett, S. J. Mooney, Effects of x-ray dose on rhizosphere studies using x-ray computed tomography, PloS one 8 (6) (2013) E67250.

[11] S. M. Walker, D. A. Schwyn, R. Mokso, M. Wicklein, T. Müller, M. Doube, M. Stampanoni, H. G. Krapp, G. K. Taylor, In vivo time-resolved microtomography reveals the mechanics of the blowfly flight motor, PLoS biology 12 (3) (2014) e1001823.

[12] F. H. Pough, T. Rogers, Experiments in x-ray irradiation of gem stones, American Mineralogist: Journal of Earth and Planetary Materials 32 (1-2) (1947) 31–43.

[13] S. Dhondt, H. Vanhaeren, D. Van Loo, V. Cnudde, D. Inzé, Plant structure visualization by high-resolution x-ray computed tomography, Trends in plant science 15 (8) (2010) 419–422.

[14] ICRP, Environmental protection - the concept and use of reference animals and plants., Tech. rep., ICRP Publication 108. Ann. ICRP 38 (4-6) (2008).

[15] F. Petruzzellis, C. Pagliarani, T. Savi, A. Losso, S. Cavalletto, G. Tromba, C. Dullin, A. Bär, A. Ganthaler, A. Miotto, et al., The pitfalls of in vivo imaging techniques: evidence for cellular damage caused by synchrotron x-ray computed micro-tomography, New Phytologist.

[16] J. Dhaene, E. Pauwels, T. De Schryver, A. De Muynck, M. Dierick, L. Van Hoorebeke, A realistic projection simulator for laboratory based

x-ray micro-ct, Nuclear Instruments and Methods in Physics Research Section B: Beam Interactions with Materials and Atoms 342 (2015) 170–178.

[17] J. Hubbell, Photon mass attenuation and energy-absorption coefficients, The International Journal of Applied Radiation and Isotopes 33 (11) (1982) 1269–1290.

[18] F. H. Attix, Introduction to radiological physics and radiation dosimetry, John Wiley & Sons, 2008.

[19] J. H. Hubbell, S. M. Seltzer, Tables of x-ray mass attenuation coefficients and mass energy-absorption coefficients 1 kev to 20 mev for elements z= 1 to 92 and 48 additional substances of dosimetric interest, Tech. rep., National Inst. of Standards and Technology-PL, Gaithersburg, MD (United States). Ionizing Radiation Div. (1995).

[20] D. Rogers, B. Faddegon, G. Ding, C.-M. Ma, J. We, T. Mackie, Beam: a monte carlo code to simulate radiotherapy treatment units, Medical physics 22 (5) (1995) 503–524.

[21] S. Agostinelli, J. Allison, K. Amako, J. Apostolakis, et al., Geant4a simulation toolkit, Nuclear instruments and methods in physics research section A: Accelerators, Spectrometers, Detectors and Associated Equipment 506 (3) (2003) 250–303.

[22] J.-F. Carrier, L. Archambault, L. Beaulieu, R. Roy, Validation of geant4, an object-oriented monte carlo toolkit, for simulations in medical physics, Medical physics 31 (3) (2004) 484–492.

[23] B. A. Faddegon, I. Kawrakow, Y. Kubyshin, J. Perl, J. Sempau, L. Urban, The accuracy of egsnrc, geant4 and penelope monte carlo systems for the simulation of electron scatter in external beam radiotherapy, Physics in Medicine & Biology 54 (20) (2009) 6151.

[24] E. Poon, F. Verhaegen, Accuracy of the photon and electron physics in geant4 for radiotherapy applications, Medical physics 32 (6Part1) (2005) 1696–1711.

[25] M. Vilches, S. Garcia-Pareja, R. Guerrero, M. Anguiano, A. Lallena, Monte carlo simulation of the electron transport through thin slabs:

A comparative study of penelope, geant3, geant4, egsnrc and mcnpx, Nuclear Instruments and Methods in Physics Research Section B: Beam Interactions with Materials and Atoms 254 (2) (2007) 219–230.

[26] J. P. Archambault, E. Mainegra-Hing, Comparison between egsnrc, geant4, mcnp5 and penelope for mono-energetic electron beams, Physics in Medicine & Biology 60 (13) (2015) 4951.

[27] L. Maigne, Y. Perrot, D. Schaart, D. Donnarieix, V. Breton, Comparison of gate/geant4 with egsnrc and mcnp for electron dose calculations at energies between 15 kev and 20 mev, Physics in Medicine & Biology 56 (3) (2011) 811.

[28] B. Masschaele, M. Dierick, D. Van Loo, M. N. Boone, L. Brabant, E. Pauwels, V. Cnudde, L. Van Hoorebeke, Hector: A 240kv micro-ct setup optimized for research 463 (1) (2013) 012012.

[29] B. Masschaele, V. Cnudde, M. Dierick, P. Jacobs, L. Van Hoorebeke, J. Vlassenbroeck, Ugct: New x-ray radiography and tomography facility, Nuclear Instruments and Methods in Physics Research Section A: Accelerators, Spectrometers, Detectors and Associated Equipment 580 (1) (2007) 266–269.

[30] W. De Boever, H. Derluyn, D. Van Loo, L. Van Hoorebeke, V. Cnudde, Data-fusion of high resolution x-ray ct, sem and eds for 3d and pseudo-3d chemical and structural characterization of sandstone, Micron 74 (2015) 15–21.

[31] C. D. Byron, A. Herrel, E. Pauwels, A. D. Muynck, B. A. Patel, Mouse hallucal metatarsal cross-sectional geometry in a simulated fine branch niche, Journal of morphology.

[32] W. Li, J. Van den Bulcke, D. Mannes, E. Lehmann, I. De Windt, M. Dierick, J. Van Acker, Impact of internal structure on water-resistance of plywood studied using neutron radiography and x-ray tomography, Construction and Building Materials 73 (2014) 171–179.

[33] K. Van Tittelboom, J. Wang, M. Araújo, D. Snoeck, E. Gruyaert, B. Debbaut, H. Derluyn, V. Cnudde, E. Tsangouri, D. Van Hemelrijck, et al., Comparison of different approaches for self-healing concrete in

a large-scale lab test, Construction and building materials 107 (2016) 125–137.

[34] M. J. Berger, J. S. Coursey, M. A. Zucker, J. Chang, Estar, pstar, and astar: Computer programs for calculating stopping-power and range tables for electrons, protons, and helium ions (version 1.2.3) (2005).